Flow Measurement and Instrumentation 53 (2017) 89–94

Contents lists available at ScienceDirect

Flow Measurement and Instrumentation

journal homepage: www.elsevier.com/locate/flowmeasinst

A portable tomography system with seventy detectors and five gamma-ray sources in fan beam geometry simulated by Monte Carlo method

A.F. Velo*, M.M. Hamada, D.V.S. Carvalho, J.F.T. Martins, C.H. Mesquita

Instituto de Pesquisas Energéticas e Nucleares – IPEN/CNEN – SP, Av. Prof. Lineu Prestes, 2242 – Cidade Universitária, São Paulo, Brazil

ARTICLE INFO

Keywords:
Monte Carlo simulation
Industrial tomography
Multiphase system
Image reconstruction

ABSTRACT

This paper describes the Monte Carlo simulation, using MCNP4C, of a portable instant non-scanning tomography containing five radioactive sources with the same activities and seventy NaI(Tl) detectors constituted of five sets of fourteen detectors, diametrically opposite to each radioactive source. The detector was validated by comparison with the experimental measurements. The full width at half maximum (FWHM) deviation between the experimental and the simulated spectra was 3.5%. A steel pipe of 17 cm×0.5 cm (diameter×thickness) containing water and two dynamic bubbles of 2 cm and 4 cm diameter were simulated. The SIRT algorithm was used to reconstruct the images. The simulated images are presented in frames. On the first frame, no bubble is observed. On the subsequent frames, the growing of the bubbles is observed, reaching the maximum diameter; after that, the bubble begins to decrease progressively, until its disappearance. The measured bubble diameters generated by simulation were 43 ± 3 mm and 27 ± 2 mm for the bubbles of 40 mm and 20 mm diameters, respectively. The spatial resolution of the proposed simulated tomography was estimated by the Modulation Transfer Function (MTF), presenting a spatial resolution of 18.3 mm and 20.2 mm for samplings at ^{137}Cs photopeak and full window, respectively.

1. Introduction

The industrial distillation system involves fast dynamic processes containing solid, liquid and gas mixtures. The distillation columns are, usually, built with steel and have large diameters and thicknesses that make their analysis unfeasible with conventional X-ray beams [1,2]. For this reason, gamma radioactive sources in the energy ranges of 317 keV (^{192}Ir), 662 keV (^{137}Cs) to ~1250 keV (^{60}Co) are preferable, instead of low X-ray energy sources [3]. While for medical tomography, the patient goes to the computed tomography system (CT), for industrial applications, the CT system should be transported up to the object (pipe or column) and, mechanically, adapted to the object setting. In addition, industrial tomography system should be adapted for different sizes of objects that are usually located in a hostile environment, containing flammable superheated materials, occasionally subjected to high internal pressure and presenting many difficulties for placing CT devices around these objects. Besides, the phenomena related to multiphase processes are usually fast, requiring high time resolution of the CT data acquisition [1,2,4]. In such case, ideally, the tomography system should be fixed and it is not necessary to move its sources and detectors around the object. Portable instant non-scanning (fourth generation like) and fifth generation tomography systems [5,6] meet these requirements. Additionally, the system should be light enough to be portable and easily installed.

Nowadays, most tomography systems do not meet these requirements and are used in laboratory environment to study and to optimize column designs and industrial processes; however, in practice, these devices are not suitable to be used in industrial plants for real time measurements.

At the University of Bergen, Norway, a high speed tomography system was developed [5,7,8], fact that served as inspiration for the portable instant non-scanning tomography designed and developed in IPEN Laboratory. The Bergen tomography system uses semiconductor detectors of CdZnTe (CZT) and five ^{241}Am sources. The CZT detectors are fixed on the printed circuit board and collimated on a complex system what makes it difficult their use for larger objects. The system was designed for a maximum pipe diameter of 80 mm [5,7,8]. Also, the use of CZT semiconductor detectors of low thickness (~1 mm) and radiation source of low energy, like the 60 keV ^{241}Am radiation, makes this tomography system not suitable to be used in the measurements of high density objects [9]. In order to be applicable, practically, in industrial plants, portable instant non-scanning tomography system, inspired in the Bergen tomography system, is being developed. However, in the industrial process plants, the analyzed objects have,

* Corresponding author.
E-mail address: afvelo@ipen.br (A.F. Velo).

http://dx.doi.org/10.1016/j.flowmeasinst.2016.09.015
Received 16 November 2015; Received in revised form 1 August 2016; Accepted 30 September 2016
Available online 01 October 2016
0955-5986/

typically, high density materials and large dimensions in their structure, such as the columns/pipes used in oil refineries, chemical, textile and petrochemical areas. Consequently, a high energy radiation source is required in order to cross the material, usually, 667 keV ^{137}Cs and ~1252 keV ^{60}Co. Therefore, dense detector material may be necessary to absorb the photons from the source [3,4]. Scintillation detectors, such as, NaI(Tl) (3.76 g/cm^3) BGO ($Bi_4Ge_3O_{12}$, 7.13 g/cm^3), LYSO ($Lu_{0.6}Y_{1.4}SiO_{0.5}$:Ce, 5.37 g/cm^3), LSO (7.35 g/cm^3) and GSO (6.71 g/cm^3) are widely used in tomography applications [3,4,10]. In our laboratory, a portable instant non-scanning tomography, that is, intrinsically, a fourth generation like tomography is being developed, comprising several sets of 2.5×5.0 cm (diameter and length) NaI(Tl) detectors and five shielding cases for radioactive sources. Each shielding case is placed diametrically opposite to a fan detector set, as showed in Fig. 1. All scintillating detectors cited meet the requirements for this project. The main criterion of choice of the NaI(Tl) was its relatively low cost compared to the other detectors suitable for the proposed application. Furthermore, it is capable to detect a large range of energies, i.e. from 60 keV ^{241}Am to ~1252 keV ^{60}Co and it has higher light output. The choice of the source to be used depends on the material densities, wall thickness and dimension of the object to be evaluated by tomography measurements. Also, the proposed tomography system may be adjusted to different dimensions of objects (columns or pipes) by changing the number of detector sets and the distance among detector, sources and object. Thus, the tomography system has the capacity of being adapted and applied for objects of different shapes and dimensions, such as, column or pipe sizes found, usually, in the industrial plants. The tomography system may be mounted on a wooden platform, which is lightweight to be replaced in future applications, according to the challenges of new geometry, dimension of the objects and application requirements..

2. Monte Carlo simulation

Monte Carlo method is a simulation tool widely used for radiation transport. This calculation technique may be applied to a wide variety of applications in the radiation field, such as radiological protection, nuclear installations, shielding and detectors modeling among several other purposes [11,12]. Its use is recommended in the first stage of the project development, in order to know its feasibility and to guide the selection of the best methodology available. Monte Carlo method is applied in this study to estimate the expected results of a portable industrial tomography, under development in our laboratory, which contains 70 NaI(Tl) detectors that surround the object in fan-beam type configuration and five source-cases that are distributed, diametrically, in front of each set of 14 detectors, as showed in Fig. 1.

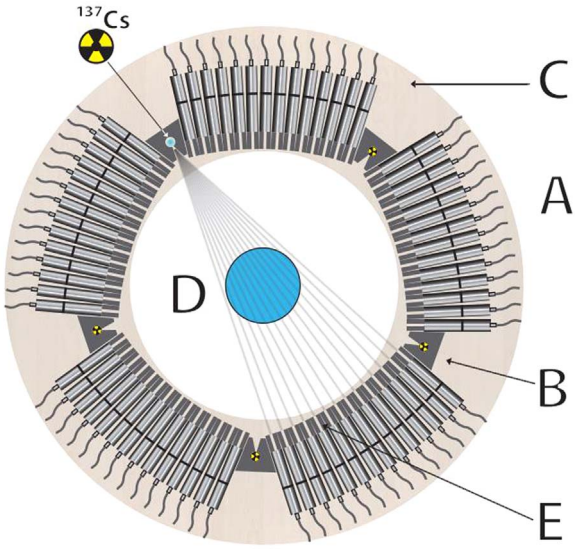

Fig. 1. Portable instant non-scanning tomography design for multiphase analysis. NaI(Tl) detectors (A), radioactive shielding case (B), wooden platform (C), the multiphase object to be analyzed (D) and detector collimator (E).

The MCNP4C (Monte Carlo N-Particle) version 4C code [13] is a general purpose Monte Carlo radiation transport designed to track different types of particles (neutrons, electrons, gamma rays), over a broad range of energies. The code obtains the solution of the problem by simulating individual particle trajectories and recording some aspects of their average behavior [14]. The process consists of following each of the many particles since their emission from a source up to reaching the energy threshold. The radiation energy is transferred to the matter by absorption, escape, physical cut-off and other processes. Probability of distributions is randomly sampled using transport data to determine the outcome, at each step of the trajectory. The quantities of interest are tallied along with estimates of the statistical precision of the results. The MCNP4C code may be used to simulate gamma-rays interactions, which comprise: (i) incoherent and coherent scattering; (ii) the possibility of fluorescent emission after photoelectric absorption; (iii) pair production with local emission of annihilation radiation and Bremsstrahlung effect [15].

When performing the mathematical simulation of NaI(Tl) detectors, in order to obtain their response curves, some corrections should be made to improve the simulation and approach the real case. Two of the main corrections are essential: the determination of the photon detection efficiency and the energy resolution, which is related to distinguish different peaks very close to each other, in the energy spectrum. Their determination has great importance when performing the identification of radionuclides or when simulating detectors that approximate the real case [14,16].

In practice, the energy resolution (R_E), as shown in Eq. (1) of the detector, is given by the full width at half maximum (FWHM) of the Gaussian peak (pulses per channel) for a given energy (E_0).

$$R_E = \frac{FWHM}{E_0} \tag{1}$$

where, R_E is the energy resolution, FWHM is the full width at half maximum of the photopeak, E_0 is the central energy of the photopeak [14,17].

Some of the effects related to the photopeak are inherent to the electronic circuit of the spectrometric system, which is not simulated by the MCNP4C. Thus, to obtain a more realistic detector response and to consider this effect in the simulation, it is necessary to achieve, experimentally, adjustment parameters of the detector energy resolution and apply a MCNP4C code function to fit Gaussian to the spectrum obtaining the suitable corrections [14].

The MCNP4C fitting technique to consider the resolution of the real detector, measured experimentally, consists of using a “ft8 geb” card into the input file of the code. The tallied energy is broadened by sampling from Gaussian, what is done by the Eq. (2).

$$f(E) = Ce^{-\left(\frac{2\sqrt{\ln 2}\,(E-E_0)}{FWHM}\right)} \tag{2}$$

where, $\boldsymbol{E}$ is the photopeak energy, $\boldsymbol{E_o}$ the energy of the tally, not broadened, and $\boldsymbol{C}$ is the normalization constant.

The energy resolution of the simulated detector may be evaluated by the Gaussian Energy Broadening (GEB) command, which is used as input to the MCNP4C code function [15]. This command is a special treatment for tallies to better simulate a physical radiation detector. For this purpose, an adjustment by non-linear least-squares procedure is applied to calculate the values of “$\boldsymbol{a}$”, “$\boldsymbol{b}$” and “$\boldsymbol{c}$” coefficients from Eq. (3) [14]. These parameters are used with GEB command.

$$FWHM = a + b\sqrt{E + cE^2} \tag{3}$$

where, $\boldsymbol{E}$ is the energy of the incident gamma ray energy (MeV). This Eq. (3) may be simplified on Eq. (4).

$$FWHM = a + b\sqrt{E} \quad (4)$$

Variations of crystal and dimensions of surrounding materials in the detectors influence the photon detection, although the simulation should be modeled with as huge accuracy as possible [18-20].

3. Experimental method

For obtaining experimentally adjustment parameters of the detector energy resolution, the experimental FWHM curve, as a function of energy, was determined by measuring two radioactive standard sources of 662 keV ^{137}Cs and 364 keV ^{131}I. The measurement was performed positioning the source under a well-defined source-detector, at a longitudinal distance of 100 mm.

The experimental efficiency measurements for the ^{137}Cs standard source were compared with simulated results under the same conditions of the experimental setup, to validate the NaI(Tl) detector simulation.

The detector simulation was based on the dimensions of the real NaI(Tl) detector used in the instant non-scanning tomography. The materials, densities and dimensions used to perform the simulation are presented in Table 1 and Fig. 2.

For the estimation of the pulse height, an F8 tally is applied to MCNP4C code [16] to obtain the deposited energy distribution per incident photon on the NaI(Tl) detector, where, for each individual history, the tally accumulates the deposited energy. In order to obtain good statistic counts, the number of histories used was 1.5×10^9.

Table 1
Materials, densities and dimensions used on the simulated NaI(Tl) detector.

Material	Density(g/cm^3)	Dimension(mm)
NaI(Tl)	3.667	Ø25.4×50.8
MgO	3.58	0.1 mm
Al	2.6989	0.5 mm
Quartz window	2.2	2 mm
Inox	7.874	1 mm

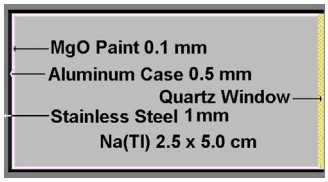

Fig. 2. Geometrical details of the NaI(Tl) detector used in simulations.

After validating the NaI(Tl) detector, the portable instant non-scanning tomography simulation was carried out to evaluate the whole system performance. For this purpose, two situations were simulated. It was assumed a 160 mm internal diameter steel column containing: (i) a ∅=40 mm spherical air bubble rising through the column filled with water (Fig. 3a), and (ii) a ∅=20 mm spherical air bubble rising through the column filled with water (Fig. 3b)..

To evaluate the portable instant non-scanning generation performance, the dimensions, detectors and the geometry were simulated as if they had been developed in order to evaluate the feasibility of the instant non-scanning tomography designed in our laboratory. The specification of the tomography simulation is presented in Table 2.

The Monte Carlo N-Particle version 4C (MCNP4C) developed by Los Alamos National Laboratory [13] was used in this work to simulate the portable instant non-scanning tomography, confirming and validating parameters, such as materials, geometry, performance and the NaI(Tl) detector to be used in the system. The expected accumulation time for each frame acquisition of the electronic that is being developed was assumed as 6.5 ms/frame. For this study, the simulation was carried out based on the tomography constituted of five sets of 14 NaI(Tl) detectors (2.5×5 cm), totalizing 70 detectors and five 662 keV ^{137}Cs sources, enclosed in tungsten shielding cases. The distance between the face of the detectors and the center of the radioactive source inside the source shielding-case was equal to 797.6 mm. For this first purpose, each detector set is constituted of fourteen NaI(Tl) detectors, positioned diametrically in the opposite side to a source shielding case (Fig. 1). All five detector sets and the five radioactive source shielding cases are mounted on a wooden platform, as shown in Fig. 1.

Table 2
Specifications of the instant non-scanning tomography.

Specifications	
Number of detectors	70
Crystal detector	NaI(Tl)
Tomography geometry	Fan-Beam
Source	Cs^{137}
Energy source	≈662 keV
Source activity	3.7×10^{10} Bq (1Ci)
History number	15 x 10^8
Source detector distance	797.6 mm
Source object distance	398.8 mm
Number of sources	5
Detector collimator thickness	50 mm
Detector collimator septum	23×5 mm^2
Source collimator septum	30×25 mm^2
Source collimator aperture angle	36^0

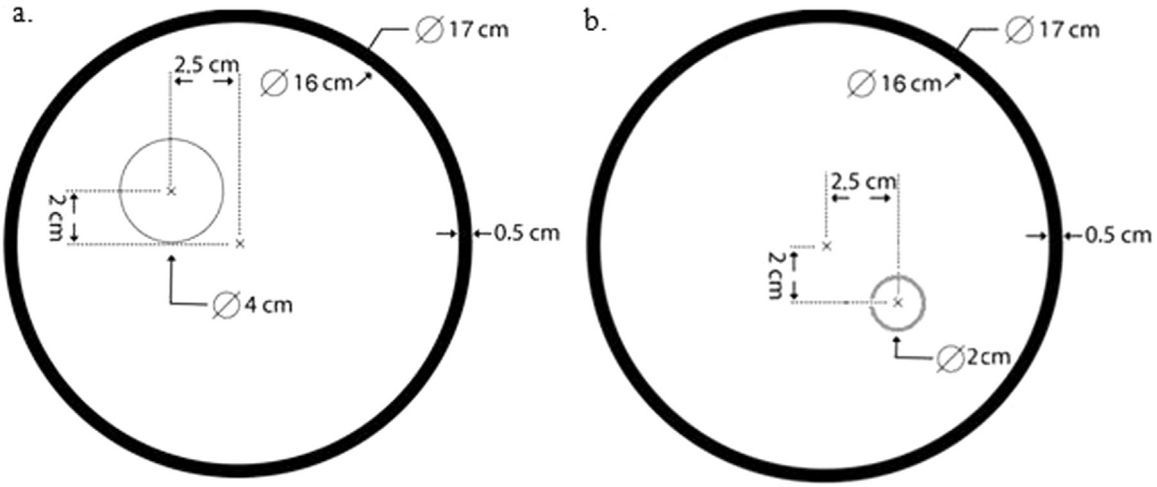

Fig. 3. The bubble models used for simulation were assumed to be spherical. The bubble on the left side has a diameter of 40 mm and the right bubble has 20 mm in diameter.

4. Image reconstruction analysis

The images reconstruction of the simulation was performed by the Simultaneous Iterative Reconstruction Technique (SIRT) [5,8]. In this work, two types of image reconstructions were carried out: (1st) open window spectrum (10–800 keV) and (2nd) at 10% photopeak window (596–728 keV), as shown on Fig. 4. The quality analysis of images obtained with open windows and images generated at the photopeak window were carried out with MTF and Root Mean Squared Error (RMSE) algorithms..

For evaluating the image reconstruction quality, it is, commonly, used the parameter called Root Mean Square Error, which is calculated by the Eq. (5) [5].

$$\mathrm{RMSE} = \sqrt{\frac{\sum_{i=1}^{N} (\mu_i - \hat{\mu}_i)^2}{N}} \quad (5)$$

where: μ_i is the observed linear attenuation coefficient value for the i^{th} pixel, $\hat{\mu}_i$ is the respective true value and N is the number of pixels.

One of the most comprehensive metric system used to measure and report spatial resolution of imaging systems is the modulation transfer function (MTF) [21,22]. The MTF provides a measure of how well the system transfers contrast across spatial frequencies [21,22].

Fourier based metrology is a prevalent approach to characterize imaging performance. This includes the MTF, which characterizes the resolution of the imaging system [21,22]. In the present work, MTF was calculated using the Edge Spread Function, commonly known as ESF parameter [21].

5. Results and discussion

The principles used in the Monte Carlo simulation and the number of histories applied showed to be very consistent, since the relative error squared (R^2) of the simulation was 0.0020 (0.2%). Errors below 0.05 are, generally, reliable for point detector [13]. The figure of merit (FOM) was 4.47×10^4, which varies according to the inverse of the square error (FOM=$1/R^2T$) [13], meaning that the bigger is the FOM, the better is the simulation.

From the experimental results using ^{131}I and ^{137}Cs, it was possible to determine the adjustment coefficients (a and b) from Eq. (4). These coefficients were: **a**=0.01363 and **b**=0.120. Fig. 5 presents the comparison of the NaI(Tl) experimental detector with the NaI(Tl) simulated detector for a 662 keV ^{137}Cs source. The comparison spectrum showed a good match between the photopeak regions. The discrepancy observed in Compton region may be due to surrounding material effect..

The FWHM for the experimental measurement was 12.6%, close to the simulated one that was 13.05%, what means a difference of about 3.5%. Due to these results, it was possible to validate the simulated NaI(Tl) detector and the MCNP4C code to perform the portable instant non-scanning tomography simulation.

MTF and the RMSE parameters are presented in Fig. 6 and Fig. 7, respectively. According to these figures, the best results were found for tomography images performed with data at the photopeak window.

The option of photopeak window compared to open window measurements has the advantage of disregarding spurious electronic

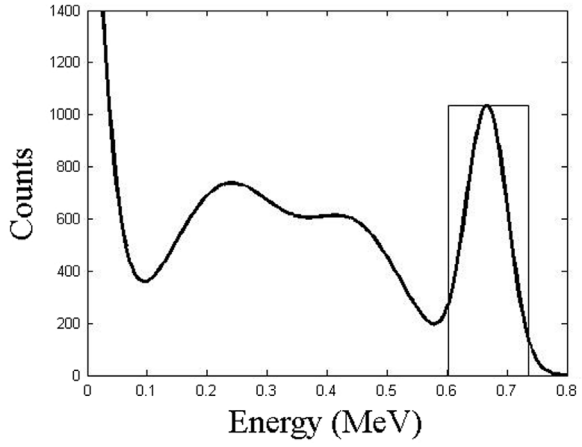

Fig. 4. ^{137}Cs spectrum with a 10% window opening at the photopeak.

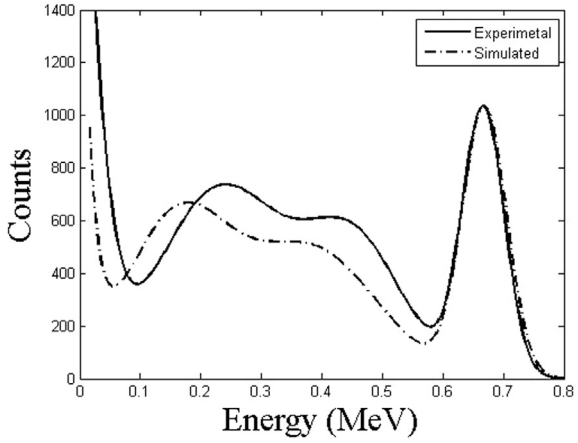

Fig. 5. Comparison between ^{137}Cs source experimental and simulated spectra.

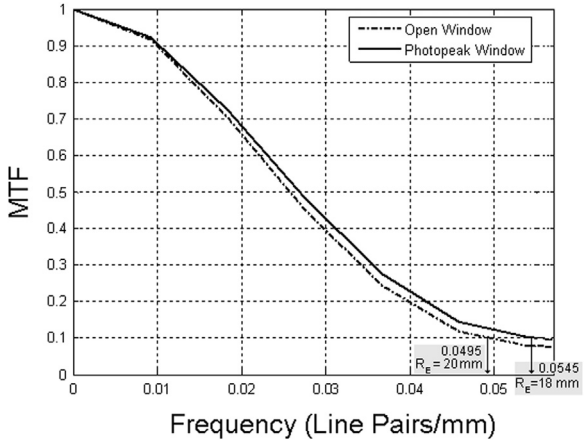

Fig. 6. Modulation transfer function analysis for the image reconstructed using the ^{137}Cs photopeak (10%) and full spectrum window.

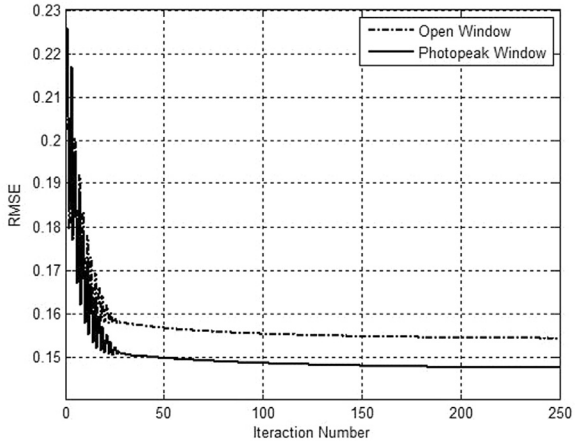

Fig. 7. Root mean square error analysis for the image reconstructed using the ^{137}Cs photopeak (10%) and full spectrum window.

signals that are not generated by the radiation source. Besides, the scattering of Compton radiation generated in one detector can reach adjacent detectors, as shown in the Fig. 8. The radiations of Compton scattering are capable of creating artifacts in the image or reducing the image resolution, as demonstrated in the Figs. 6 and 7. Practically all emission tomography systems used in nuclear medicine, such as PET, SPECT and Gamma Camera employ the measurement system centered on photopeak window.

MTF analysis was carried out in order to obtain the spatial resolution of the portable instant non-scanning tomography. Fig. 6 presents the MTF along the frequencies. Conventionally, the spatial resolution is estimated as the inverse of the value at 10% of MTF curve [23]. From Fig. 6, the frequency for an MTF equal to 0.1 is 0.0545 line pairs per mm, for sampling at photopeak region and 0.0495 line pairs per mm, for full window sampling; thus, the tomography system has a spatial resolution of 18.3 mm and 20.2 mm for photopeak and full window samplings, respectively.

The estimated RMSE value was 0.148 for the 40 mm bubble tomogram, calculated by Eq. (5). Better image reconstructions are obtained when RMSE value is low. The RMSE algorithm compares the experimental linear attenuation coefficients with the respective theoretical values. The obtained RMSE value of 0.148 endorses the methodology applied, namely, SIRT algorithm and Monte Carlo simulation.

All projections obtained by Monte Carlo simulation were reconstructed in 32×32 pixels matrix using the SIRT algorithm, assuming the relaxation parameter equal.to 0.19 and iteration number as being 100. As non-scanner tomography requires fast image reconstruction,

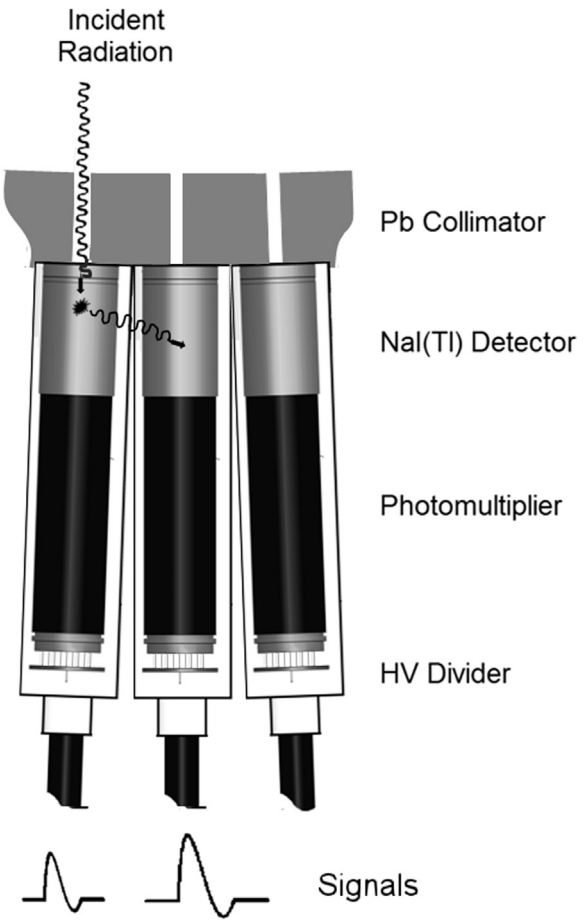

Fig. 8. Demonstration of the advantage to use the photopeak window measurement. Some photons from the radiation source can interact by Compton scattering process and the scattered photon can reach other detectors generating signals in the adjacent detectors, causing undesirable artifacts in the reconstructed image and also decreasing the spatial resolution.

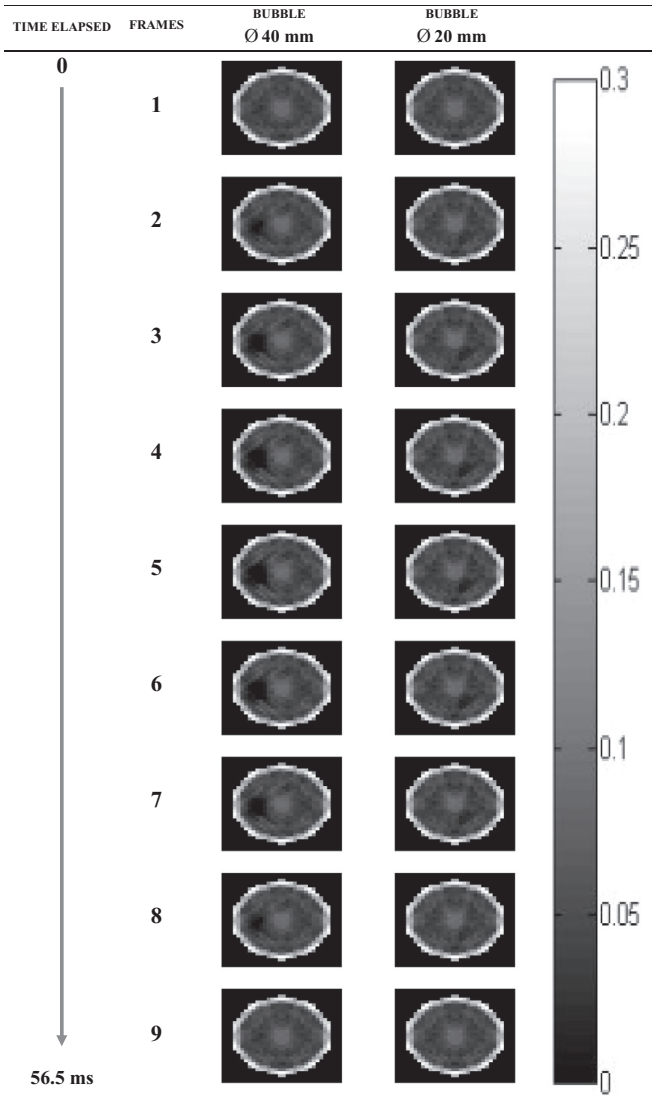

Fig. 9. Simulated bubble reconstructed image rising along the steel column of 40 mm diameter bubble (a) and 20 mm diameter bubble (b).

the relaxation parameter of 0.19 was chosen since, for this proposal, it was the value that converged faster to the linear attenuation coefficient. The number iteration greater than 100 did not present significant improvement, as shown in Fig. 7.

The two different bubbles, in a steel pipe filled with water, were generated and evaluated using two dynamic air bubbles of 40 mm and 20 mm diameters. Fig. 9 presents the evolution of the 40 mm and 20 mm diameter bubbles flow, rising through the steel pipe (Figs. 3a and b). The images of 40 mm diameter bubble were best defined, while for 20 mm diameter bubble, the images were not so distinguished, suggesting that the bubble of 20 mm was close to the limit of the spatial resolution, as it may be inferred from Fig. 6. It should be emphasized that the studies were carried out at the photopeak window due to better reconstruction images obtained, compared to full spectrum.

As shown in Fig. 9, it is possible to observe the passage of the bubbles in the tomographic sampling plan. All nine images (frames) were totally sampled in 56.5 ms or 6.2 ms/frame, which was enough time to observe the passage of the bubbles along the pipe. The bubbles reach their major size at frame #5 (Fig. 9). After that, the images decreased up to their disappearance.

The diameter of the bubbles was calculated by MatLab® r2013b, obtaining dimensions of ∅ 43 ± 3 mm and ∅ 27 ± 2 mm that are close to the theoretical bubble sizes of ∅=40 mm and ∅=20 mm, respectively.

Fig. 10. 3D image reconstruction of the simulated bubbles (40 and 20 mm diameter).

Fig. 10 presents the 3D reconstruction of the proposed simulated examples, where it can be observed the 40 and 20 mm diameter air bubble rising in an aqueous multiphase system.

For this studied tomography system configuration, using five sets of fourteen NaI(Tl) detectors (2.54 cm diameter × 5.0 cm length detectors) and five radioactive shielding cases, the maximum object diameter to be evaluated is limited to 20 mm. However, the proposed tomography configuration has the advantage of easily re-arrange and adapt to a larger object size, by increasing the number of detector sets. Also, the shielding cases are projected for shielding a large energy range of radioactive sources, from 60 keV ^{241}Am to ~1250 keV ^{60}Co, and the sources may be easily changed. For objects with larger wall thickness, higher energy source is required.

Concerning the resolution parameter, practically, there is no difference between the two ways of sampling. The low spatial resolution found was due to low number of sampling projections: only five and few detectors used per projection, i.e. fourteen detectors. Despite the low resolution compared to other tomography devices, the major objective of this proposed portable instant non-scanning system is the temporal resolution, with acquisition electronic spending only 6.5 ms per sampling.

6. Conclusions

The simulation of the proposed tomography showed that the system has suitable capacity to distinguish several structures in the multiphase systems, differentiated in approximated 6.5 ms per data acquisition. Simulated results demonstrated the feasibility of the development of the instantaneous scanning tomography containing seventy NaI(Tl) detectors and boards of multichannel acquisition system. RMSE value of 0.148 demonstrated that the reconstruction image is representative of the true image, presenting suitable accuracy. According to RMSE analysis, SIRT algorithm reconstruction was suitable for tomography image reconstruction of the dynamic bubbles. The spatial resolution estimated by the MTF method was of 18.3 mm and 20.2 mm for photopeak and open window samplings and temporal resolution estimated as being 6.5 ms per sampling.

Acknowledgments

The authors would like to express their gratitude to CNEN (Brazilian Nuclear Energy Commission Grant number 2016/240), CNPq (The Brazilian National Research Council Grant nos. 305210/2013-0 and 308560/2015-9) and FAPESP (Foundation for Research Support of the State of São Paulo Grant number 2012/22705-3) for financial support A.F. Velo thanks to the CNEN, D.V.S. Carvalho and J.F.T. Martins to the CNPQ for the fellowships.

References

[1] S.B. Kumar, M.P. Dudukovic, Computer-assisted gamma and X-ray tomography: application to multiphase flow, in: J. Chaouki, F. Larachi, M.P. Dudukovic (Eds.), Non-Invasive Monitoring of Multiphase Flows, Elsevier, Amsterdam, The Netherlands, 1997, p. 48. (Chapter 2).
[2] J.C. Gamiob ISMAILA, Tomography for multi-phase flow measurement in the oil industry, Flow Meas. Instrum. 16 (2002) 145–155.
[3] G.A. Johansen, P. Jackson, Radioisotope Gauges for Industrial Process Measurements, John Wiley & Sons, England, 2004.
[4] P.A.S. Vasquesz, C.H. Mesquita, G.A.C. Leroux, M.M. Hamada, Methodological analysis of gamma tomography system for large random packed columns, Appl. Radiat. Isot. 68 (2010) 658–661.
[5] R. Maad, G.A. Johansen, Experimental analysis of high-speed gamma-ray tomography performance, Meas. Sci. Technol. 19 (2008) 1–10.
[6] F. Fischer, D. Hoppe, E. Schleicher, G. Mattausch, H. Flaske, R. Bartel, U. Hampel, An ultra-fast electron beam x-ray tomography scanner, Meas. Sci. Technol 19 (2008) 1–11.
[7] R. Maad, B.T. Hjertaker, G.A. Johansen, Ø. Olsen, Dynamic characterization of a high speed gamma-ray tomography, Flow Meas. Instrum. 21 (2010) 538–545.
[8] B.T. Hjertaker, R. Maad, E. Schuster, O.A. Almås, G.A. Johansen, A data acquisition and control system for high-speed gamma-ray tomography, Meas. Sci. Technol. 19 (2008) 1–9.
[9] G.A. Johansen, T. Frøystein, B.T. Hjertaker, Ø. Olsen, A dual sensor flow imaging tomographic system measurement, Sci. Technol. 7 (1996) 297–307.
[10] C.M. Pepin, P. Bérard, A.L. Perrot, C. Pepin, D. Houde, R. Lecomte, C.L. Melcher, H. Dautet, Properties of LYSO and recent LSO scintillators for phoswich PET detectors, IEEE Trans. Nucl. Sci. 51 (2004) 789–795.
[11] C.M. Salgado, L.E.B. Brandão, R. Schirru, C.M.N.A. Pereira, R. Ramos, A.X. Silva, Prediction of volume fractions in three-phase flows using nuclear technique and artificial neural network, Appl. Radiat. Isot. 67 (2009) 1812–1818.
[12] M.C.F. Moreira, C.C. Conti, R. Schirru, A new NaI(Tl) four-detector layout for field contamination assessment using artificial neural networks and the Monte Carlo method for system calibration, Nucl. Instrum. Methods Phys. Res. 621 (2010) 302–309.
[13] MCNP4C User Manual, Version 4C, 2000. Radiation Safety Information Computational Center (RSICC), Los Alamos National Laboratory, University of California, USA. Available at ⟨http//mcnp-green.lanl.gov⟩.
[14] C.M. Salgado, L.E.B. Brandão, R. Schirru, C.M.N.A. Pereira, C.C. Conti, Validation of a NaI(Tl) detector's model developed with MCNP-X code, Prog. Nucl. Energy 59 (2012) 19–25.
[15] D.B. Pelowitz, MCNP-X TM User's Manual, Version 2.5.0., 2005, LA-CP-05-0369, Los Alamos National Laboratory.
[16] A. Jehouani, R. Ichaoui, M. Boulkneir, Study of the NaI(Tl) efficiency by Monte-Carlo method, Appl. Radiat. Isot. 53 (4-5) (2000) 887–891.
[17] M.H. Hadizadeh Yazdi, A.A. Mowlavi, M.N. Thompson, H. Miri Hakimabad, Proper shielding for Na(Tl) detectors in combined neutron-gamma fields using MCNP, Nucl. Instrum. Methods Phys. 522 (2004) 447–454.
[18] M. Hashem, P. Hamed, V.N. Alireza, Nonlinear response function of 3×3 in NaI scintillation detector, Asian J. Exp. Sci. 21 (1) (2007) 1–12.
[19] T. Nakamura, Monte Carlo calculation of peak efficiencies of Ge(Li) and pure Ge detectors to volume sources and comparison with environmental radioactivity measurement, Nucl. Instrum. Methods 205 (1983) 211–218.
[20] O. Sima, Monte Carlo simulation versus semiempirical calculation of autoabsorption actors for semiconductor detector calibration in complex geometries, Prog. Nucl. Energy 24 (1990) 327–336.
[21] Sl Richard, D.B. Husarik, G. Yadava, S.N. Murphy, E. Samei, Towards task-based assessment of CT performance: system and object MTF across different reconstruction algorithms, Med. Phys. 39 (2012) 4115–4122.
[22] E. Samei, M.J. Flynn, D.A. Reimann, A method for measuring the presampled MTF of digital radiographic systems using an edge test device, Med. Phys. 25 (1) (1998) 102–113.
[23] D.J. Dowsett, P.A. Kenny, R.E. Johnston. The Physics of Diagnostic Imaging, Hodder Arnold Ed., second ed., 2006.